

Experimental Consequences of the S-wave $\cos(k_x) \cdot \cos(k_y)$ Superconductivity in the Iron-Pnictides

Meera M. Parish,^{1,2} Jiangping Hu,³ and B. Andrei Bernevig^{1,2}

¹*Department of Physics, Princeton University, Princeton, NJ 08544*

²*Princeton Center for Theoretical Science, Princeton University, Princeton, NJ 08544*

³*Department of Physics, Purdue University, West Lafayette, IN 47907*

(Dated: 9:23pm, February 6, 2020)

The experimental consequences of different order parameters in iron-based superconductors are theoretically analyzed. We consider both nodeless and nodal order parameters, with an emphasis on the $\cos(k_x) \cdot \cos(k_y)$ nodeless order parameter recently derived by two of us¹. We analyze the effect of this order parameter on the spectral function, density of states, tunneling differential conductance, penetration depth, and the NMR spin relaxation time. This extended *s*-wave symmetry has line-zeros in between the electron and hole pockets, but they do not intersect the two Fermi surfaces for moderate doping, and the superconductor is fully gapped. However, this suggests several quantitative tests: the exponential decay of the penetration depth weakens and the density of states reveals a smaller gap upon electron or hole doping. Moreover, the $\cos(k_x) \cdot \cos(k_y)$ superconducting gap is largest on the smallest (hole) Fermi surface. For the $1/T_1$ NMR spin relaxation rate, the inter-band contribution is consistent with the current experimental results, including a (non-universal) T^3 behavior and the absence of a coherent peak. However, the intra-band contribution is considerably larger than the inter-band contributions and still exhibits a small enhancement in the NMR spin relaxation rate right below T_c in the clean limit.

Introduction – The recent discovery of iron-based superconductors with a transition temperature as high as 55K has stimulated a flurry of experimental activity^{2,3,4,5,6,7,8,9,10}. However, a conclusive observation of the pairing symmetry still remains elusive, with both nodal and nodeless order parameters reported in experimental observations.

Numerical and analytic research suggests that the antiferromagnetic exchange coupling between Fe sites is strong^{11,12,13}. Owing to As-mediated hopping, antiferromagnetic exchange exists not only between the nearest neighbor (NN) Fe sites, but also between next nearest neighbor (NNN) sites. Moreover, the NNN coupling strength J_2 is stronger than the NN coupling strength J_1 . The $J_1 - J_2$ model produces half-filled magnetic physics consistent with experimental neutron data¹⁴. A nematic magnetic phase transition has been predicted in this model^{15,16}, consistent with the experimental observation of a structural transition preceding the spin density wave (SDW) formation. This model suffers, however, from an important deficiency - it is an insulator whereas the real material is an, albeit bad, metal. We, however, believe that the spin-spin interaction insight is important to the physics of the iron-pnictides.

In a recent paper¹, two of us added electron itineracy to the problem and studied a $t - J_1 - J_2$ model *without* band renormalization. We found that the singlet-forming $J_1 - J_2$ interaction gives rise to four possible pairing symmetries: $\cos(k_x) \pm \cos(k_y)$, $\sin(k_x) \cdot \sin(k_y)$ and $\cos(k_x) \cdot \cos(k_y)$. The last two are strongly preferred from an interaction standpoint when $J_2 > J_1$, but only $\cos(k_x) \cdot \cos(k_y)$ matches the symmetry of the iron-pnictide Fermi surface: it is maximal around $(0,0)$, $(\pi,0)$, $(0,\pi)$, (π,π) - the location of the Fermi surfaces in the unfolded one-iron per site Brillouin zone.

Although we used a specific, two band model for our calculation¹, our results are completely independent of any model, *as long as* the dominating interaction is next-nearest neighbor J_2 and the Fermi surfaces are located close to the aforementioned spots in the Brillouin zone. Some order parameters (such as $d_{xy} = \sin(k_x) \cdot \sin(k_y)$ and others) mismatch the Fermi surface symmetry and can be discarded. We note that $\cos(k_x) \cdot \cos(k_y)$ changes sign between the electron and hole pockets in the Brillouin zone. In this sense, it resembles the order parameter proposed by Mazin through weak-coupling general arguments¹⁷. At moderate doping, our gap is isotropic within the same Fermi surface, while changing sign between electrons and hole pockets, but at relatively high doping $\cos(k_x) \cdot \cos(k_y)$ exhibits some anisotropy even within the same Fermi surface.

Neutron measurements have found antiferromagnetic stripe order of Fe moments ranging from $0.26\mu_B$ in NaOFeAs¹⁸ and $0.36\mu_B$ ¹⁹ in LaOFeAs to $0.8\mu_B$ in CeOFeAs²⁰ and SrFe₂As₂²¹. A magnetic moment of $0.8\mu_B$ is fully consistent with a purely localized spin-one Heisenberg model. While a magnetic moment of $0.3\mu_B$ is smaller than what is expected in a purely localized spin-one system, it is rather larger than what can be obtained in a truly weak coupling theory. We point out that, due to imperfect nesting, weak coupling theory requires large values of $U/t \sim 4$ to explain even small magnetic moments ($< 0.2\mu_B$), clearly outside the weak-coupling limit²². Considering these facts, together with the rather high resistivity of the iron-pnictides, we find that the experimental evidence paints a picture of the iron-pnictides as being at moderate interaction couplings. Thus, moderate to strong coupling models can provide an accurate qualitative description of the observed phenomena. In fact, the $t - J_1 - J_2$ model predicts the right physics of

the parent state SDW as well as the $\cos(k_x) \cdot \cos(k_y)$ order parameter.

In this paper we focus on the experimental properties of several superconducting order parameters proposed in the iron-pnictides, with particular emphasis on the $\cos(k_x) \cdot \cos(k_y)$ order parameter. We look at a simplified two-band superconducting model and obtain the spectral function, density of states, tunneling differential conductance, penetration depth and NMR spin relaxation time. We stress the important point that the $\cos(k_x) \cdot \cos(k_y)$ order parameter features lines of zeroes at $(\pm\pi/2, k_y)$ and $(k_x, \pm\pi/2)$, as in Fig. 1 (obviously, irrespective of its harmonic form, any order parameter changing sign between the electron and hole Fermi surfaces must have zero-lines). Thus, at low doping, the hole and electron Fermi pockets are far away from the zero lines of the order parameter and the superconductivity is nodeless.

Close to half-filling, we find that the $\cos(k_x) \cdot \cos(k_y)$ order parameter exhibits an exponentially decaying $\delta\lambda(T) = \lambda(T) - \lambda(0)$, where $\lambda(T)$ is the penetration depth at temperature T , as expected for a nodeless superconductor. However, upon doping, the gap on the Fermi surface varies in magnitude: for electron doping, the gap decreases on the electron pocket and increases on the hole pocket. The penetration depth is sensitive to the smallest gap in the system, and hence exhibits a weakened exponential decay upon doping. This could explain the conflicting values of the gap parameters obtained by fitting the penetration depth experiments to the BCS exponential form^{23,24,25}. In the unlikely event that the system remains superconducting at very large doping, then the Fermi surfaces will cross the line of zeroes of $\cos(k_x) \cdot \cos(k_y)$ at around 35% doping, and cause $\delta\lambda(T)$ to become linearly dependent on T .

We also calculate the NMR spin relaxation rate $1/T_1$ of the bare superconductor and find that it factorizes into inter- and intra-band contributions. While, for the $\cos(k_x) \cdot \cos(k_y)$ order parameter, the inter-band contribution to the NMR spin relaxation rate does *not* exhibit a coherence peak, the intra-band contribution is larger than the inter-band contribution and still exhibits an enhancement right below T_c owing to its fully gapped s -wave nature. Adding the two contributions we find that, although the coherence peak for $\cos(k_x) \cdot \cos(k_y)$ is smaller than for a sign-preserving gap such as, for example, $|\cos(k_x) \cdot \cos(k_y)|$, it is still present due to the intra-band contribution. The coherence peak can be strongly reduced if the intra-band scattering is stronger than inter-band scattering or if the samples are strongly disordered. If the As structure factor $A(\mathbf{q})$ is taken into account, the inter-band contribution is severely reduced due to the fact that $A(\mathbf{q}) = \cos(q_x/2)\cos(q_y/2)$ is zero close to the wavevector difference between the electron and hole Fermi surfaces: $\mathbf{q} = (\pm\pi, 0), (0, \pm\pi)$. The As structure factor also reduces the overall coherence peak by smearing the intra-band contribution.

Model – We approximate the typical iron-based material by a two-dimensional square lattice of Fe atoms,

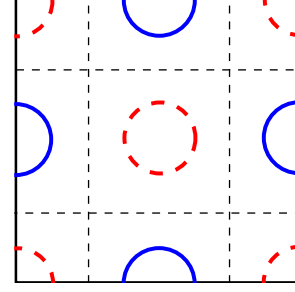


FIG. 1: Schematic diagram of the Fermi surfaces in the iron-pnictides at half-filling in the unfolded Brillouin zone $-\pi \leq k_x \leq \pi, -\pi \leq k_y \leq \pi$. The dashed (red) and solid (blue) curves correspond to the hole and electron Fermi surfaces, respectively. The dashed lines mark the nodal lines at $(\pm\pi/2, k_y)$ and $(k_x, \pm\pi/2)$ for the $\cos(k_x) \cdot \cos(k_y)$ order parameter proposed in Ref. 1.

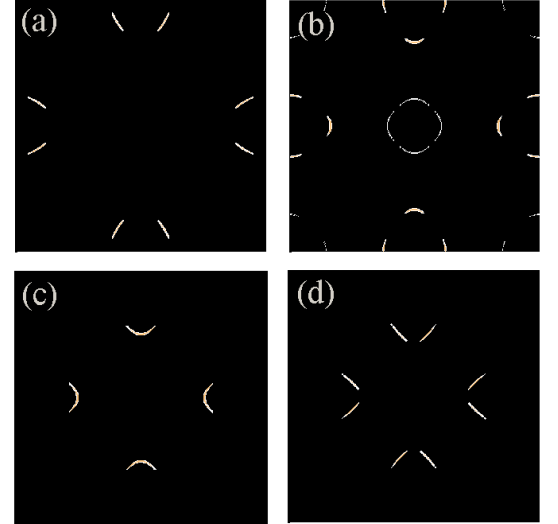


FIG. 2: Behavior of the spectral function $A(\mathbf{k}, w)$ in an interval about the Fermi energy ($-0.02 < w < 0.02$) across the unfolded Brillouin zone $-\pi \leq k_x \leq \pi, -\pi \leq k_y \leq \pi$ for gap parameter $\Delta_0 = 0.1$. Panels (a) and (b) depict the $s_{x^2+y^2}$ and d_{xy} order parameters, respectively, both at chemical potential $\mu = 1.6$. The $s_{x^2+y^2}$ order parameter is shown in panels (c) and (d) for the higher electron doping values $\mu = 2$ and $\mu = 2.2$, respectively. For these high doping values, the $s_{x^2+y^2}$ superconductor has become nodal. The lighter regions illustrate the ungapped portions of the Fermi surface.

since the superconductivity has been shown to be associated with the FeAs layer. To capture the degeneracy of the d_{xz} and d_{yz} orbitals on the Fe atoms, we use the two-orbital per site model proposed by Ref. 22. Although this description is only valid in the case of an unphysically large crystal field splitting, we particularize to this model for analytic simplicity. The kinetic part of the Hamiltonian is written:

$$H_0 = \sum_{\mathbf{k}\sigma} \psi_{\mathbf{k}\sigma}^\dagger \begin{pmatrix} \epsilon_x(\mathbf{k}) - \mu & \epsilon_{xy}(\mathbf{k}) \\ \epsilon_{xy}(\mathbf{k}) & \epsilon_y(\mathbf{k}) - \mu \end{pmatrix} \psi_{\mathbf{k}\sigma} \quad (1)$$

Here, $\psi_{\mathbf{k}\sigma}^\dagger = (c_{1,\mathbf{k},\sigma}^\dagger, c_{2,\mathbf{k},\sigma}^\dagger)$ is the creation operator for spin σ electrons in the two orbitals $(1, 2) = (d_{xz}, d_{yz})$, μ is the chemical potential, and the matrix elements are

$$\begin{aligned} \epsilon_x(\mathbf{k}) &= -2t_1 \cos k_x - 2t_2 \cos k_y - 4t_3 \cos k_x \cos k_y \\ \epsilon_y(\mathbf{k}) &= -2t_2 \cos k_x - 2t_1 \cos k_y - 4t_3 \cos k_x \cos k_y \\ \epsilon_{xy}(\mathbf{k}) &= -4t_4 \sin k_x \sin k_y \end{aligned} \quad (2)$$

While Eq. (1) is only a simplified version of the true band structure of the material, it produces Fermi pockets that resemble those predicted by density functional theory (see Fig. 1). The eigenvalues of (1) are:

$$E_\pm = \epsilon_+ - \mu \pm \sqrt{\epsilon_-^2 + \epsilon_{xy}^2} \quad (3)$$

where $\epsilon_\pm = (\epsilon_x \pm \epsilon_y)/2$. In the following, we take $t_1 = -1$, $t_2 = 1.3$, and $t_3 = t_4 = -0.85$. The undoped compound, where there are two electrons per site, corresponds to $\mu = 1.54$.

We now assume that the interacting part of the Hamiltonian induces singlet pairing between electrons within each orbital, but we make no further assumptions about the form of the interaction or the pairing mechanism. Then we introduce pairing gaps $\Delta_{1,2}$ for each orbital and we write down the mean-field effective Hamiltonian $H(\Delta_1, \Delta_2) = \sum_{\mathbf{k}} \Psi(\mathbf{k})^\dagger B(\mathbf{k}) \Psi(\mathbf{k})$, where

$$B(\mathbf{k}) = \begin{pmatrix} \xi_x(\mathbf{k}) & \Delta_1(\mathbf{k}) & \epsilon_{xy}(\mathbf{k}) & 0 \\ \Delta_1^*(\mathbf{k}) & -\xi_x(\mathbf{k}) & 0 & -\epsilon_{xy}(\mathbf{k}) \\ \epsilon_{xy}(\mathbf{k}) & 0 & \xi_y(\mathbf{k}) & \Delta_2(\mathbf{k}) \\ 0 & -\epsilon_{xy}(\mathbf{k}) & \Delta_2^*(\mathbf{k}) & -\xi_y(\mathbf{k}) \end{pmatrix} \quad (4)$$

with $\xi_x = \epsilon_x - \mu$, $\xi_y = \epsilon_y - \mu$, and we have used the four-component spinor $\Psi(\mathbf{k}) = (c_{1,\mathbf{k},\uparrow}, c_{1,-\mathbf{k},\downarrow}^\dagger, c_{2,\mathbf{k},\uparrow}, c_{2,-\mathbf{k},\downarrow}^\dagger)$. We neglect inter-orbital pairing in order to make the problem analytically tractable. This is also reasonable because two of us proved in Ref. 1 that, at least for the case of the $t - J_1 - J_2$ model (and hence for the most important gap we will be focusing on $-\cos(k_x) \cdot \cos(k_y)$), the inter-orbital pairing expectation value is negligible even in the case of strong Hund's rule coupling.

The symmetry of the superconducting order parameter $\Delta(\mathbf{k})$ has two possible d -wave types¹: $d_{x^2-y^2} \sim \Delta_0(\cos k_x - \cos k_y)$ and $d_{xy} \sim \Delta_0 \sin k_x \sin k_y$, and three possible s -wave types¹: $s_{x^2+y^2} \sim \Delta_0(\cos k_x + \cos k_y)$, $s_{x^2y^2} \sim \Delta_0 \cos k_x \cos k_y$, as well as the constant gap (s_0) which is not allowed in the $t - J_1 - J_2$ model but can obviously appear in other interacting models. The C_4 symmetry of the underlying lattice maps $k_x \leftrightarrow k_y$ and $d_{xz} \leftrightarrow d_{yz}$. Hence for all the pairing symmetries described above we have $\Delta_1(k_x, k_y) = \Delta_2(k_y, k_x)$, except for $d_{x^2-y^2}$ where $\Delta_1(k_x, k_y) = -\Delta_2(k_x, k_y)$.¹ The $d_{x^2-y^2}$, d_{xy} and $s_{x^2+y^2}$ pairing symmetries are nodal while the other pairing symmetries are nodeless. We now proceed to analyzing the experimental consequences of these pairing symmetries.

Spectral Function, Density of States and Tunneling Differential Conductance – The single-particle density of states (DOS) can be written as:

$$\begin{aligned} \mathcal{N}(\omega) &\equiv \sum_{\mathbf{k}} \mathcal{A}(\mathbf{k}, \omega) \\ &= -\frac{1}{\pi} \sum_{\mathbf{k}} \Im[\mathcal{G}_{11}(\mathbf{k}, \omega + i\delta) + \mathcal{G}_{33}(\mathbf{k}, \omega + i\delta)] \end{aligned} \quad (5)$$

where $\mathcal{A}(\mathbf{k}, \omega)$ is the spectral function and $\mathcal{G}_{11}(\mathbf{k}, \omega + i\delta)$ and $\mathcal{G}_{33}(\mathbf{k}, \omega + i\delta)$ are the electron components of the superconducting Green's function. Generally, we find:

$$\begin{aligned} \mathcal{A}(\mathbf{k}, \omega) &= \frac{\epsilon_{xy}^2(2\omega - \xi_x - \xi_y) - (\omega + \xi_y)(\omega^2 - \xi_x^2 - \Delta_1^2) - (\omega + \xi_x)(\omega^2 - \xi_y^2 - \Delta_2^2)}{E_1^2 - E_3^2} \\ &\times \left[\frac{1}{2E_3}(\delta(E_3 - \omega) - \delta(E_3 + \omega)) - \frac{1}{2E_1}(\delta(E_1 - \omega) - \delta(E_1 + \omega)) \right] \end{aligned} \quad (6)$$

where E_1 and E_3 are the positive eigenvalues of the matrix $B(\mathbf{k})$ in (4) (see Ref. 1). For the case where $\Delta_1 = \Delta_2 = \Delta$ (valid except for the $d_{x^2-y^2}$ pairing symmetry), we have the simplified form:

$$\mathcal{A}(\mathbf{k}, \omega) = \frac{\omega + E_-(\mathbf{k})}{2E_-^\Delta(\mathbf{k})} [\delta(E_-^\Delta(\mathbf{k}) - \omega) - \delta(E_-^\Delta(\mathbf{k}) + \omega)] + \frac{\omega + E_+(\mathbf{k})}{2E_+^\Delta(\mathbf{k})} [\delta(E_+^\Delta(\mathbf{k}) - \omega) - \delta(E_+^\Delta(\mathbf{k}) + \omega)] \quad (7)$$

with $E_\pm^\Delta(\mathbf{k}) = \sqrt{E_\pm^2(\mathbf{k}) + \Delta^2(\mathbf{k})}$. This resembles two independent single-band superconductors with the energy

dispersions E_\pm .

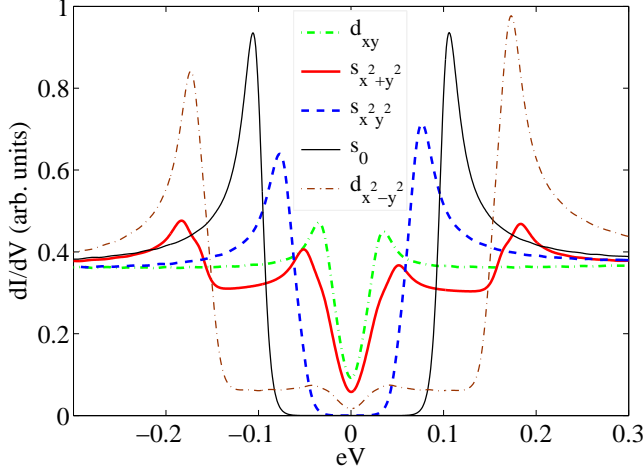


FIG. 3: Tunneling differential conductance $dI/dV \propto -\int \mathcal{N}(\omega) n'_F(\omega - eV)$ as a function of bias voltage eV measured with respect to the Fermi energy, where the temperature $k_B T = 0.005$, the chemical potential $\mu = 1.6$, and the gap size $\Delta_0 = 0.1$ for all the different pairing symmetries.

The spectral function at the Fermi energy $\mathcal{A}(\mathbf{k}, \omega = 0)$ contains information about the nodal structure for each pairing symmetry, as shown in Fig. 2. The $s_{x^2+y^2}$ pairing symmetry exhibits nodes on the Fermi surface for all dopings when $k_x = (\pm\pi - k_y), (\pm\pi + k_y)$ and thus only the hole Fermi pockets are fully gapped. The d_{xy} pairing symmetry also has nodes for all doping, but in this case they occur when $k_{x,y} = 0, \pm\pi$ and so all of the Fermi surfaces are gapless. The $d_{x^2-y^2}$ pairing symmetry (not shown) exhibits nodes on the Fermi surface of the hole pockets for any doping and it has a similar effect on the electron pockets as the $s_{x^2+y^2}$ pairing symmetry which is the dominant pairing symmetry that we found in Ref. 1. The $s_{x^2+y^2}$ pairing only has nodes on the Fermi surface above a critical doping $\mu \simeq 2$ since the zeros of the gap lie at $k_{x,y} = \pm\pi/2$. For $\mu < 2$, the electron Fermi surfaces are fully gapped, like the hole Fermi surfaces. In principle, information about the form of the $s_{x^2+y^2}$ gap can be obtained through ARPES. In the *folded* Brillouin Zone, there are two hole pockets at the Γ point. A $\cos(k_x) \cdot \cos(k_y)$ order parameter predicts a *larger* gap for the smaller hole Fermi surface and *smaller* gap for the larger hole Fermi surface.

Tunneling measurements access the local DOS to a first approximation. Specifically, if we assume that both the tunneling matrix element and the probe DOS are momentum independent, then the tunneling differential conductance is²⁶:

$$\frac{dI}{dV} \propto -\int_{-\infty}^{\infty} \mathcal{N}(\omega) n'_F(\omega - eV) \quad (8)$$

where eV is the bias voltage of the tunneling probe and $n'_F(E) \equiv \partial n_F(E)/\partial E$ is the derivative of the Fermi function. In the limit of zero temperature, we obviously recover the DOS. From Fig. 3, we see that a fully-gapped

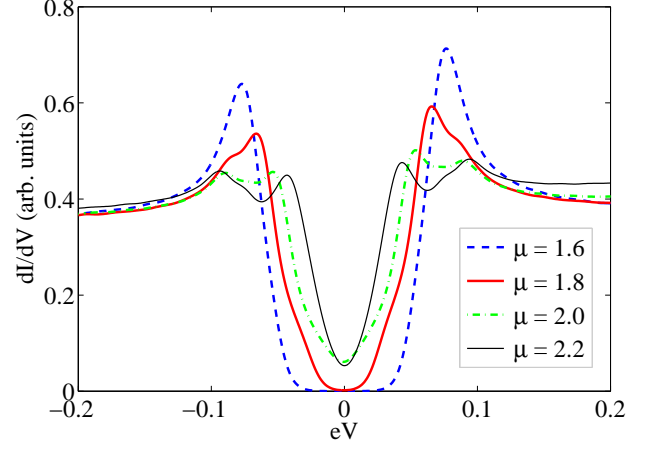


FIG. 4: Tunneling differential conductance dI/dV as a function of bias voltage eV for the pairing symmetry $s_{x^2+y^2}$ at different dopings. Like Fig. 3, $k_B T = 0.005$ and $\Delta_0 = 0.1$.

Fermi surface yields a corresponding gap in dI/dV at low energies, while for a gapless Fermi surface, the DOS grows quasi-linearly with energy at $\omega = 0$, a text-book result. In particular, $s_{x^2+y^2}$ ($d_{x^2-y^2}$) pairing produces a four-peak structure in the differential conductance because in this case each band sees a different order parameter: the hole (electron) Fermi surfaces are fully gapped while the electron (hole) Fermi surfaces are gapless.

Focussing on $s_{x^2+y^2}$ pairing¹ (Fig. 4), we find that the differential conductance smoothly evolves from fully gapped to gapless behavior with increasing doping, as expected. Moreover, when the doping is large, we obtain a four-peak structure similar to $s_{x^2+y^2}$ pairing, because we also have a fully-gapped hole Fermi surface and a partially-gapped electron Fermi surface. While it is likely that the material cannot be doped high enough so that the $s_{x^2+y^2} = \cos(k_x) \cdot \cos(k_y)$ superconductor becomes gapless (the material will most likely exit the superconducting state at such high dopings), we believe that the predictions above, in particular the evolution of the differential conductance with doping, could be used in careful experiments to falsify this order parameter.

Penetration depth – Measurements of the penetration depth in the Fe-based superconductors were the first to suggest that the Fermi surfaces are fully gapped^{23,24,25}. The experiments show an exponentially temperature decay of $\delta\lambda(T) = \lambda(T) - \lambda(0)$. Among the different order parameters studied here, such a scenario is only consistent with $s_{x^2+y^2}$ symmetry at low doping or a constant s -wave gap. We now obtain the penetration depth for the bare two band superconductor with generic $\Delta_{1,2}$ gaps.

To obtain the penetration depth, we perform a text-book exercise. We write the FeAs model in real space and introduce a gauge field via the Peierls substitution $c_{i,\alpha}^\dagger c_{j,\beta} \rightarrow c_{i,\alpha}^\dagger \exp(i \int_i^j \vec{A} \cdot d\vec{l}) c_{j,\beta}$ where α, β are the two orbital indices. We pick a Landau gauge $\vec{A} = A\hat{x}$ and expand to second order in A , thus obtaining $H(A)$. The sec-

ond order term in A is the diamagnetic current while the first order term gives the paramagnetic current, whose response must be calculated in linear response. We have:

$$H(A) \approx H(0) - \sum_i (j_x^p(i) A_x(i) + \frac{1}{2} j_x^d(i) A_x(i)^2) \quad (9)$$

hence

$$j_x(i) = -\frac{\delta H(A)}{\delta A_x(i)} = j_x^p(i) + j_x^d(i) A_x(i) \quad (10)$$

Using translational invariance, the expectation value of the diamagnetic current in the ground state is:

$$\begin{aligned} \langle j_x^d(i) \rangle &= \frac{1}{N_s} \sum_i \langle j_x^d(i) \rangle \\ &= -\frac{1}{V} \sum_{\mathbf{k}} \frac{\partial^2 \epsilon_x}{\partial k_x^2} \langle c_{\mathbf{k},1}^\dagger c_{\mathbf{k},1} \rangle + \frac{\partial^2 \epsilon_y}{\partial k_x^2} \langle c_{\mathbf{k},2}^\dagger c_{\mathbf{k},2} \rangle \\ &\quad + \frac{\partial^2 \epsilon_{xy}}{\partial k_x^2} \langle c_{\mathbf{k},1}^\dagger c_{\mathbf{k},2} + c_{\mathbf{k},2}^\dagger c_{\mathbf{k},1} \rangle \end{aligned} \quad (11)$$

where the expectation values of the above operators are computed in the appropriate ground state. The param-

agnetic current is obtained through a correlation function in linear response: $j_x^p(\mathbf{q}, \omega) = Q_{xx}(\mathbf{q}, \omega) A_x(\mathbf{q}, \omega)$:

$$Q_{xx}^d(\mathbf{q}, i\nu_n) = \frac{1}{N} \int_0^\beta d\tau e^{i\nu_n \tau} \langle j_x^p(\mathbf{q}, \tau) j_x^p(-\mathbf{q}, 0) \rangle \quad (12)$$

This is the vacuum polarization. For the FeAs metal (*not* the superconductor), this is explicitly given by:

$$\begin{aligned} Q_{xx}(\mathbf{q}, i\nu_n) &= -\frac{1}{V\beta} \sum_{\mathbf{k}, m} \times \\ &Tr \left(J_x(\mathbf{k}) G(i\omega_m + i\nu_n, \mathbf{k} + \frac{\mathbf{q}}{2}) J_x(\mathbf{k}) G(i\omega_m, \mathbf{k} - \frac{\mathbf{q}}{2}) \right) \end{aligned} \quad (13)$$

where $\omega_m = (2m+1)\pi T$ is a fermionic matsubara frequency while $\nu_n = 2n\pi T$ is a bosonic one. J_x is the current operator, which is expressed as $\partial H / \partial k_x$ in the metal. For the response to a magnetic field, the limit that has to be taken is, upon analytic continuation, $i\nu_n \rightarrow \omega + i\delta$, $\omega = 0$, $\mathbf{q} \rightarrow 0$. The opposite limit $\omega \rightarrow 0$, $\mathbf{q} = 0$ gives the response to an electric field, and hence the electrical conductivity. After tedious but straightforward algebra, we obtain for the FeAs metal:

$$Q_{xx}(\mathbf{q} \rightarrow 0, \omega = 0) = -\frac{2}{V} \sum_{\mathbf{k}} \left(\frac{\partial E_+}{\partial k_x} \right)^2 \frac{\partial n(E_+)}{\partial E_+} + \left(\frac{\partial E_-}{\partial k_x} \right)^2 \frac{\partial n(E_-)}{\partial E_-} + \frac{8(n(E_+) - n(E_-))}{(E_+ - E_-)^3} \left(\epsilon_{xy} \frac{\partial \epsilon_-}{\partial k_x} - \epsilon_- \frac{\partial \epsilon_{xy}}{\partial k_x} \right)^2 \quad (14)$$

The overall factor of 2 reflects the spin multiplicity. Besides the usual paramagnetic expression (first two terms in Eq. (14)), the cross-orbital exchange introduces an extra second term. We have checked that this paramagnetic term completely cancels the diamagnetic ground state expectation value, as is required for a metal. We performed the same calculation in the superconductor. The charge matrix operator in our superconductor is:

$$J_0 = \begin{pmatrix} 1 & 0 & 0 & 0 \\ 0 & -1 & 0 & 0 \\ 0 & 0 & 1 & 0 \\ 0 & 0 & 0 & -1 \end{pmatrix} \quad (15)$$

The current operator uses *only* the kinetic part of the

kinetic Hamiltonian and is obtained from the continuity equation, giving:

$$J_x = \frac{1}{2} \left\{ \frac{\partial H(\Delta_1 = 0, \Delta_2 = 0)}{\partial k_x}, J_0 \right\} \quad (16)$$

where $\{, \}$ is the anticommutator. The penetration depth $\delta\lambda(T) = \lambda(T) - \lambda(0)$ is proportional to the current-current correlation function which uses the Green's function of the superconductor, not written here due to space restrictions. For the case where $\Delta_1 = \Delta_2$, we can write the current-current correlation function as:

$$\begin{aligned} Q_{xx}(q \rightarrow 0, \omega = 0) &= -\sum_{\mathbf{k}} 2 \left[\left(\frac{\partial E_+}{\partial k_x} \right)^2 n'_F(E_+^\Delta) + \left(\frac{\partial E_-}{\partial k_x} \right)^2 n'_F(E_-^\Delta) \right] \\ &+ \frac{1}{\xi_+ (\xi_-^2 + \epsilon_{xy}^2)^{3/2}} \left(\epsilon_{xy} \frac{\partial \xi_-}{\partial k_x} - \xi_- \frac{\partial \epsilon_{xy}}{\partial k_x} \right)^2 \times \left[(2n_F(E_+^\Delta) - 1) \frac{\xi_+ E_+ + \Delta^2}{E_+^\Delta} - (2n_F(E_-^\Delta) - 1) \frac{\xi_+ E_- + \Delta^2}{E_-^\Delta} \right] \end{aligned} \quad (17)$$

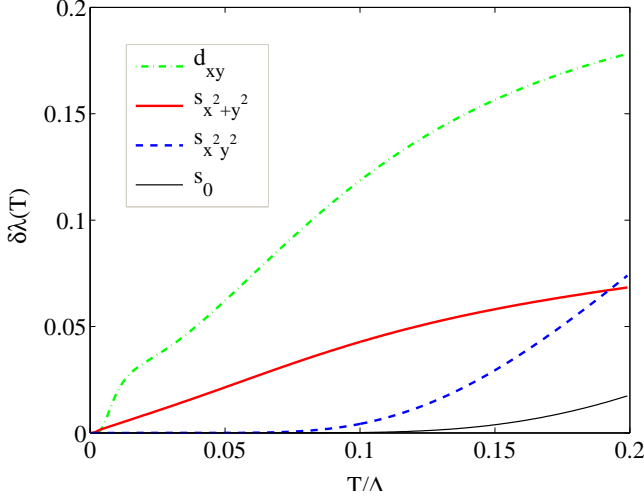


FIG. 5: Penetration depth $\delta\lambda(T) = \lambda(T) - \lambda(0) \propto Q_{xx}(\mathbf{q} \rightarrow 0, \omega = 0)$ close to zero temperature for different pairing symmetries at doping $\mu = 1.6$ and gap size $\Delta_0 = 0.1$. The d_{xy} curve has been reduced by a factor of two for clarity. The $d_{x^2-y^2}$ pairing symmetry (not shown) will have a similar low temperature behavior to the d_{xy} and $s_{x^2+y^2}$ curves.

We see that the cross-orbital exchange introduces an extra term, similar to the case of the FeAs metal, but the largest contribution to the temperature dependence arises from the first term. We have obtained the expression of the current-current correlation function for general $\Delta_1 \neq \Delta_2$, but we do not include it for space reasons.

We now plot the low temperature dependence of the penetration depth $\delta\lambda(T) = \lambda(T) - \lambda(0)$ for different superconducting gaps (see Fig. 5). As expected, the nodal order parameters exhibit a linear T dependence (in the absence of impurities) while the nodeless order parameters exhibit an exponentially decaying penetration depth. However, as shown in Fig. 6, one qualitative feature is that the $\cos(k_x) \cdot \cos(k_y)$ order parameter exhibits, upon doping, a weakened exponential decay, a signature that the gap on the electron (hole) surface *decreases* upon electron (hole) doping. This is a direct consequence of the existence of a line of zeroes in between the electron and hole pockets. Above some critical doping, the exponential decay of $\delta\lambda(T)$ in the $\cos(k_x) \cdot \cos(k_y)$ superconductor becomes linear (Fig. 6), a sign that the superconductor has become gapless.

NMR Spin Relaxation Rate and the Coherence Peak – Existing experimental results for the NMR spin relaxation time T_1 at first sight suggest a d -wave symmetry for the order parameter, because there is no coherence peak in $1/T_1$ at T_c and $1/T_1$ scales like T^3 just below T_c ^{27,28,29,30}. These results pose a big challenge for the s -wave pairing symmetry or any other nodeless order parameter. In the case of a $\cos(k_x) \cdot \cos(k_y)$ order parameter, although we find that the coherence peak due to inter-band contributions is non-existent, the intra-band contributions still give a coherence peak, although smaller

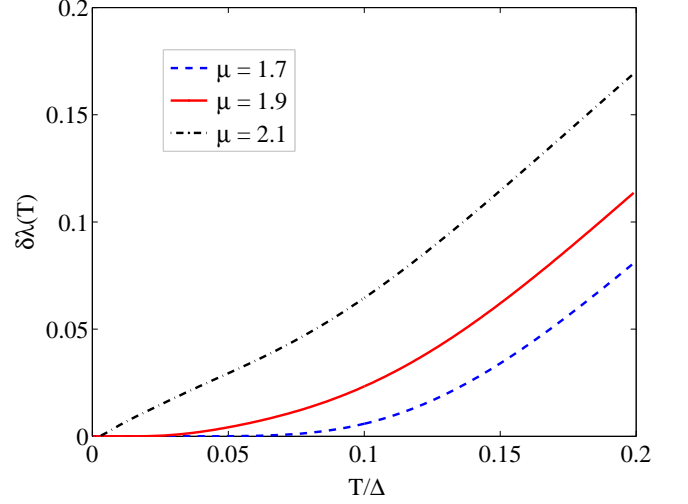


FIG. 6: Penetration depth $\delta\lambda(T) = \lambda(T) - \lambda(0)$ for the pairing symmetry $s_{x^2y^2}$ at different dopings, where $\Delta_0 = 0.1$.

and flatter than in a pure s -wave scenario. Neglecting the intra-band contributions (which could be justified if the broadenings of the inter- and intra-band contributions are different) can then explain the observed lack of the coherence peak, but in general a small coherence peak should be seen in cleaner samples.

The NMR measurements have been performed on different atoms in the pnictides, including ^{19}F and ^{75}As . Experimentally, there is no major difference between the $1/T_1$ results on these two atoms. This also poses a challenge to the NMR theories because the structure factors for F and As are different: while the structure factor for F is roughly isotropic in the transferred momentum \mathbf{q} , the As structure factor is roughly $A(\mathbf{q}) = \cos(q_x/2) \cos(q_y/2)$ due to the placement of the As atoms in the center of the Fe unit cell (although the As are out of plane, we believe the $\cos(q_x/2) \cos(q_y/2)$ faithfully represents the structure factor). Hence, for small Fermi electron and hole pockets, the As NMR measurements should not be sensitive to the inter-band contributions, whose transfer wavevector $(\pi, 0)$ is suppressed by the structure factor.

The NMR spin relaxation rate at temperature T is defined as:

$$R = \frac{1}{T_1 T} = -\frac{1}{2\pi} \lim_{\omega_0 \rightarrow 0} \frac{\Im[K_{+-}(\omega_0)]}{\omega_0} \quad (18)$$

where

$$K_{+-}(\omega_0) = \sum_{\mathbf{q}} A(\mathbf{q}) \xi^{+-}(\mathbf{q}, \omega_0) \quad (19)$$

$\xi^{+-}(\mathbf{q}, \omega_0)$ is the spin susceptibility in the superconducting state and $A(\mathbf{q})$ is the structure factor. Since we are dealing with singlet superconductivity we have:

$$\xi^{+-} = \frac{1}{2}(\xi^{xx} + \xi^{zz}) = \xi^{zz} \quad (20)$$

where ξ^{zz} is now much simpler due to the fact that the S^z spin matrix in a superconductor is the identity matrix:

$$K_{+-}(\omega_0) = \frac{1}{V^2\beta} \sum_{\omega_n, \mathbf{k}_1, \mathbf{k}_2} A(\mathbf{k}_2 - \mathbf{k}_1) \times \text{Tr}[G(\mathbf{k}_1, i(\omega_n + \omega_0))G(\mathbf{k}_2, i\omega_n)] \quad (21)$$

After Matsubara sums, analytic continuation, and taking the imaginary part, for the pure gap case $\Delta_1 = \Delta_2 = \Delta$, we obtain the following formula for $1/(T_1T)$,

$$\begin{aligned} \frac{1}{T_1T} = \sum_{\mathbf{k}_1, \mathbf{k}_2} A(\mathbf{k}_2 - \mathbf{k}_1) & \left[\left(1 + \frac{\Delta(\mathbf{k}_1)\Delta(\mathbf{k}_2) + E_+(\mathbf{k}_1)E_+(\mathbf{k}_2)}{E_+^\Delta(\mathbf{k}_1)^2} \right) \frac{\partial n}{\partial E_+^\Delta(\mathbf{k}_1)} \delta(E_+^\Delta(\mathbf{k}_2) - E_+^\Delta(\mathbf{k}_1)) \right. \\ & + \left(1 + \frac{\Delta(\mathbf{k}_1)\Delta(\mathbf{k}_2) + E_-(\mathbf{k}_1)E_-(\mathbf{k}_2)}{E_-^\Delta(\mathbf{k}_1)^2} \right) \frac{\partial n}{\partial E_-^\Delta(\mathbf{k}_1)} \delta(E_-^\Delta(\mathbf{k}_2) - E_-^\Delta(\mathbf{k}_1)) \\ & \left. + 2 \left(1 + \frac{\Delta(\mathbf{k}_1)\Delta(\mathbf{k}_2) + E_+(\mathbf{k}_1)E_-(\mathbf{k}_2)}{E_+^\Delta(\mathbf{k}_1)^2} \right) \frac{\partial n}{\partial E_+^\Delta(\mathbf{k}_1)} \delta(E_-^\Delta(\mathbf{k}_2) - E_+^\Delta(\mathbf{k}_1)) \right] \quad (22) \end{aligned}$$

Following Bulut and Scalapino,³¹ we phenomenologically take disorder into consideration by broadening the Kronecker delta functions, e.g. $\pi\delta(E_-^\Delta(\mathbf{k}_2) - E_+^\Delta(\mathbf{k}_1)) = -\Gamma/((E_-^\Delta(\mathbf{k}_2) - E_+^\Delta(\mathbf{k}_1))^2 + \Gamma^2)$. This simple inclusion of disorder works well towards explaining the experimental data in the cuprate case, and merely serves as a cutoff for the singularities in the density of states. The first two terms in Eq. (22) represent the intra-band contribution and the third term represents the inter-band contribution, which is a contribution between the electron and hole pockets. We perform the momentum integrals by Monte Carlo evaluation: this is necessary due to the fact that we keep the strong-coupling superconductivity and do not make the usual approximation which transforms the 4 momentum integrals and the delta function into an easy one dimensional integral over energies close to the Fermi surface.

The inter-band and intra-band contributions have different behaviors as a function of temperature. Owing to the fact that for \mathbf{k}_1 on the hole Fermi surface and \mathbf{k}_2 on the electron Fermi surface, $\Delta(\mathbf{k}_1) > 0$ while $\Delta(\mathbf{k}_2) < 0$, we expect the inter-band contribution to lack a coherence peak around the superconducting transition temperature, which is indeed what we find below.

We first consider a uniform structure factor, i.e. $A(\mathbf{q}) = 1$. In Fig. 7, we contrast the inter-band contribution for the $s_{x^2y^2}$ pairing symmetry with that of its absolute value, i.e. $|\cos(k_x) \cdot \cos(k_y)|$, which does not exhibit a sign change between the hole and electron pockets. Clearly, the former case does not possess a coherence peak, while the latter does, as expected. In Fig. 8, we plot the intra-band contribution and the total $1/T_1$ for both cases. We see that, compared to the absolute value case, the coherence peak in $1/T_1$ is suppressed in the $\cos(k_x) \cdot \cos(k_y)$ case.

Using the structure factor $A(\mathbf{q})$ for As atoms (Fig. 9) we find that the inter-band component of the to-

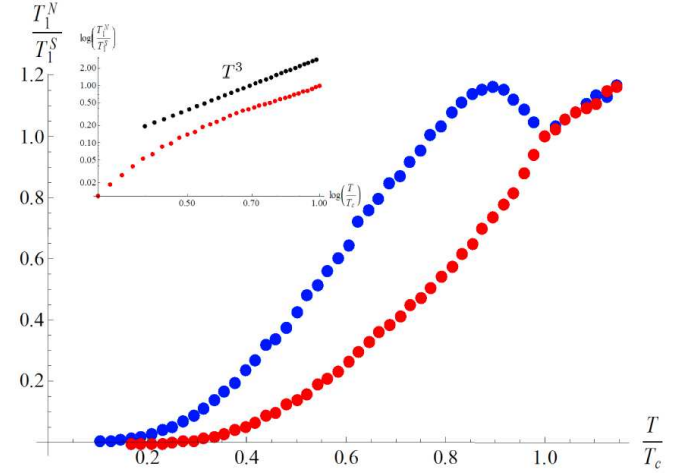


FIG. 7: Monte-Carlo calculation of the (normalized) inter-band contributions to the NMR coherence peak for $\Delta_0 \cos(k_x) \cdot \cos(k_y)$ (red) and a fixed-sign version of it, $\Delta_0 |\cos(k_x) \cdot \cos(k_y)|$ (blue). We choose a large $\Delta_0 = |t_1|/5$ and $\Delta_0/T_c = 2$. The broadening factor is $\Gamma = T_c/5$, and $\mu = 1.8$ corresponding to 18% electron doping. Inset: Temperature dependence of the NMR spin relaxation time for $\Delta_0 \cos(k_x) \cos(k_y)$ (red). The structure factor here is taken to be $A(q) = 1$.

tal NMR spin relaxation rate *decreases*. While for $A(\mathbf{q}) = 1$ the inter-band contribution represented about 1/6 of the overall spin relaxation rate, for $A(\mathbf{q}) = \cos(q_x/2)\cos(q_y/2)$ that ratio decreases to about 1/12. We hence find that the intra-band contribution is dominant in the case of the As structure factor. However, we also find that the structure factor *reduces the intra-band coherence peak*, to give an overall result plotted in Fig. 9.

Finally, we find that the NMR relaxation rates for the nodal superconductors d_{xy} and $s_{x^2+y^2}$, depicted in

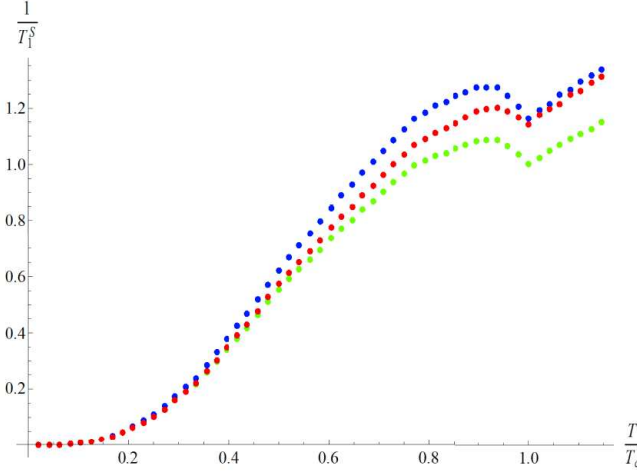


FIG. 8: Monte-Carlo calculation of the (normalized) intra-band contributions to the NMR coherence peak for the $\Delta_0 \cos(k_x) \cdot \cos(k_y)$ (green) gap (the intra-band contribution is equal for the two gaps $\Delta_0 \cos(k_x) \cdot \cos(k_y)$ and $\Delta_0 |\cos(k_x) \cdot \cos(k_y)|$). The total, intra plus inter band contributions for $\Delta_0 \cos(k_x) \cdot \cos(k_y)$ (red) and $\Delta_0 |\cos(k_x) \cdot \cos(k_y)|$ (blue) are also plotted. We can see that the intra-band contribution is hence much larger than the inter-band contribution for both these order parameters, and hence the $\Delta_0 \cos(k_x) \cdot \cos(k_y)$ gap should exhibit a small coherence peak. We choose a large $\Delta_0 = |t_1|/5$ and $\Delta_0/T_c = 2$. The broadening factor is $\Gamma = T_c/5$, and $\mu = 1.8$ corresponding to 18% electron doping. The structure factor here is taken to be $A(q) = 1$.

Fig. 10, lack a coherence peak as expected.

We predict that future experiments will see a small coherence peak resulting from the intra-band contribution. Our results show that, barring different scattering rates for inter- and intra-band scattering, the overall intra-band contribution to the NMR relaxation rate is roughly a factor of 5 times larger than the inter-band contribution. This can also be argued on general grounds, provided that the hypothesis of weak-coupling theories and LDA (i.e. there is a quasi-nesting of the electron and hole Fermi surfaces in the parent material) is correct. Upon doping with either electrons or holes, either the electron or hole Fermi surfaces will become considerably larger than the other one. This means that the inter-band contribution to the NMR spin relaxation rate diminishes: it of course vanishes if one could, theoretically, deplete one of the Fermi pockets. Meanwhile, the intra-band contribution should, on general grounds, remain roughly constant upon doping because the overall size of the sum of the Fermi surfaces is relatively constant. All these general arguments are supported by our explicit calculation.

A few other remarks about the NMR spin relaxation rates are in order: (i) The observed T^3 temperature dependence of $1/T_1$ cannot be viewed as evidence against s -wave pairing symmetries. In fact, the temperature dependence just below T_c is very sensitive to the ratio

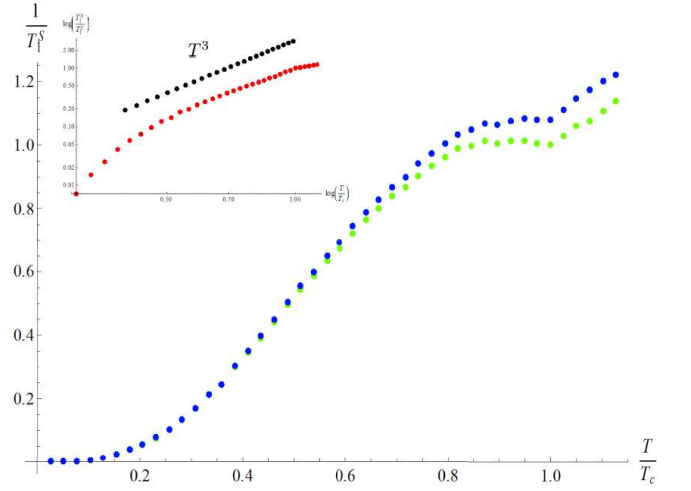


FIG. 9: Monte-Carlo calculation of the (normalized) intra-band contributions to the NMR coherence peak for the $\Delta_0 \cos(k_x) \cdot \cos(k_y)$ (green) gap, with the structure factor $A(\mathbf{q}) = \cos(q_x/2) \cos(q_y/2)$ for the As atoms. The total, intra plus inter band contributions for $\Delta_0 \cos(k_x) \cdot \cos(k_y)$ (blue) are also plotted. The coherence peak is diminished from the case when $A(\mathbf{q}) = 1$, plotted previously. Inset: Temperature dependence of the inter band contribution. We choose a large $\Delta_0 = |t_1|/5$ and $\Delta_0/T_c = 2$. The broadening factor is $\Gamma = T_c/5$, and $\mu = 1.8$ corresponding to 18% electron doping.

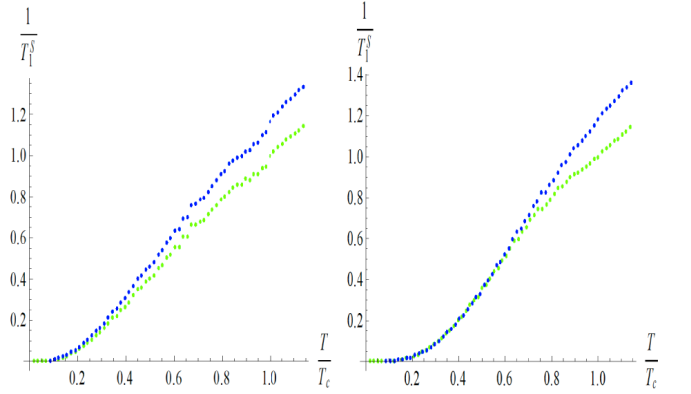


FIG. 10: Monte-Carlo calculation of the (normalized) intra-band (green) and total (blue) contributions to the NMR coherence peak for the $\Delta_0 \sin(k_x) \sin(k_y)$ (left) and $\Delta_0 (\cos(k_x) + \cos(k_y))$ gap. These are nodal superconductors and lack a coherence peak. We choose a large $\Delta_0 = |t_1|/5$ and $\Delta_0/T_c = 2$. The broadening factor is $\Gamma = T_c/5$, and $\mu = 1.8$ corresponding to 18% electron doping. The structure factor here is taken to be $A(q) = 1$.

$\Delta/k_B T_c$. We find that the T^3 behavior can be obtained by choosing $\Delta/k_B T_c \sim 2$ for our large gap value, and the power of the temperature dependence can increase even further by increasing this ratio. (ii) Although we predict that there should be a coherence peak in the clean limit, impurities can efficiently reduce the coherence peak in a two-band system. A weak inter-band impurity scat-

tering but strong intra-band scattering can suppress the coherence peak. This has been investigated in MgB_2 ³² where the coherence peak is also not easily observed experimentally³³. Since the superconductivity in Fe-based superconductors is created by doping, it is reasonable to assume that disorder is stronger than that in MgB_2 . To observe the coherence peak, we require a very clean sample. (iii) Our calculation is based on a two-band model. This model can be over-simplified when one tries to use it to predict quantitative experimental measurements. For example, the detailed shape of Fermi surfaces and its doping dependence may not be quantitatively accurate. Therefore, the predictions in this paper with regard to doping concentration should be viewed as qualitative.

Conclusion – We have calculated the spectral function, the DOS, the tunneling differential conductance, the penetration depth, and the NMR spin relaxation rate for different superconducting order parameters in the iron-pnictides. We have emphasized that the nodal structure of the $s_{x^2-y^2}$ order parameter will result in a qualitative change in these experimental observables with increasing doping, as the superconductor crosses over from gapped to gapless. Thus, one can in principle probe the existence of this pairing symmetry in the iron-pnictides by analyzing the behavior of the spectral function, the DOS

and the penetration depth as a function of doping. For the $1/T_1$ NMR spin relaxation rate, if only the inter-band contribution is considered, our theoretical results are consistent with the current experimental results, including the T^3 behavior and the absence of a coherence peak. However, by including the intra-band contribution, a small coherence peak at the transition temperature will be present in a clean sample although it is smaller than that in a sign-unchanged s -wave.

Note – During the completion of this work, we became aware of two recent papers that also calculate the spin-lattice relaxation rate for the $s_{x^2-y^2}$ order parameter in the iron-pnictides^{34,35}, and another recent paper that considers the experimental consequences of two different pairing symmetries³⁶.

Acknowledgements BAB wishes to thank P.W. Anderson, S. Sondhi, N.P. Ong, Z. Hasan, A. Yazdani, for discussions and comments. MMP and BAB are especially grateful to David Huse for fruitful discussions. JPH thanks Pengcheng Dai, S. Kivelson, X. Tao, E. W. Carlson, G. Q. Zheng, I.I. Mazin, H. Yao, for important discussion. JPH was supported by the National Science Foundation under grant No. PHY-0603759. MMP and BAB are supported by PCTS fellowships.

-
- ¹ K. Seo, B. A. Bernevig, and J. Hu, arXiv:0805.2958.
 - ² Y. Kamihara, T. Watanabe, M. Hirano, and H. Hosono, J. Am. Chem. Soc. **130**, 3296 (2008).
 - ³ H. Takahashi, K. Igawa, K. Arii, Y. Kamihara, M. Hirano, and H. Hosono, Nature **453**, 376 (2008).
 - ⁴ Z.-A. Re, J. Yang, W. Lu, W. Yi, G.-C. Che, X.-L. Dong, L.-L. Sun, and Z.-X. Zhao, arXiv:0803.4283.
 - ⁵ G. F. Chen, Z. Li, G. Li, J. Zhou, D. Wu, J. Dong, W. Z. Hu, P. Zheng, Z. J. Chen, J. L. Luo, et al., arXiv:0803.0128.
 - ⁶ X. H. Chen, T. Wu, G. Wu, R. H. Liu, H. Chen, and D. F. Fang, arXiv:0803.3603.
 - ⁷ H.-H. Wen, G. Mu, L. Fang, H. Yang, and X. Zhu, Europhys. Lett. **82**, 17009 (2008).
 - ⁸ M. Rotter, M. Tegel, and D. Johrendt, arXiv:0805.4630.
 - ⁹ K. Sasmal, B. Lv, B. Lorenz, A. Guloy, F. Chen, Y. Xue, and C. W. Chu, arXiv:0806.1301.
 - ¹⁰ G. F. Chen, Z. Li, G. Li, W. Z. Hu, J. Dong, X. D. Zhang, P. Zheng, N. L. Wang, and J. L. Luo, arXiv:0806.1209.
 - ¹¹ F. Ma, Z.-Y. Lu, and T. Xiang, arXiv:0806.3526.
 - ¹² T. Yildirim, arXiv:0804.2252.
 - ¹³ Q. Si and E. Abrahams, arXiv:0804.2480.
 - ¹⁴ H. A. Mook, Y. Sidis, B. Fauqué, V. Balédent, and P. Bourges, arXiv:0802.3620.
 - ¹⁵ C. Fang, H. Yao, W.-F. Tsai, J. Hu, and S. A. Kivelson, Phys. Rev. B **77**, 224509 (2008).
 - ¹⁶ C. Xu, M. Mueller, and S. Sachdev, arXiv:0804.4293.
 - ¹⁷ I. I. Mazin, D. J. Singh, M. D. Johannes, and M. H. Du, arXiv:0803.2740.
 - ¹⁸ Y. Chen, J. W. Lynn, J. Li, G. Li, G. F. Chen, J. L. Luo, N. L. Wang, P. Dai, C. dela Cruz, and H. A. Mook, arXiv:0807.0662.
 - ¹⁹ C. de la Cru, Q. Huang, J. W. Lynn, J. Li, W. R. II, J. L. Zarestky, H. A. Mook, G. F. Chen, J. L. Luo, N. L. Wang, et al., Nature **453**, 899 (2008).
 - ²⁰ J. Zhao, Q. Huang, C. de la Cruz, S. Li, J. W. Lynn, Y. Chen, M. A. Green, G. F. Chen, G. Li, Z. Li, et al., arXiv:0806.2528.
 - ²¹ J. Zhao, W. R. II, J. W. Lynn, G. F. Chen, J. L. Luo, N. L. Wang, J. Hu, and P. Dai, arXiv:0807.1077.
 - ²² S. Raghu, X.-L. Qi, C.-X. Liu, D. Scalapino, and S.-C. Zhang, arXiv:0804.1113.
 - ²³ L. Malone, J. D. Fletcher, A. Serafin, A. Carrington, N. D. Zhigadlo, Z. Bukowski, S. Katrych, and J. Karpinski, arXiv:0806.3908.
 - ²⁴ K. Hashimoto, T. Shibauchi, T. Kato, K. Ikada, R. Okazaki, H. Shishido, M. Ishikado, H. Kito, A. Iyo, H. Eisaki, et al., arXiv:0806.3149.
 - ²⁵ C. Martin, R. T. Gordon, M. A. Tanatar, M. D. Vannette, M. E. Tillman, E. D. Mun, P. C. Canfield, V. G. Kogan, G. D. Samolyuk, J. Schmalian, et al., arXiv:0807.0876.
 - ²⁶ O. Fischer, M. Kugler, I. Maggio-Aprile, C. Berthod, and C. Renner, Rev. Mod. Phys. **79**, 353 (2007).
 - ²⁷ K. Matano, Z. Ren, X. Dong, L. Sun, Z. Zhao, G. Zheng, et al., arXiv:0806.0249.
 - ²⁸ H.-J. Grafe, D. Paar, G. Lang, N. J. Curro, G. Behr, J. Werner, J. Hamann-Borrero, C. Hess, N. Leps, R. Klingeler, et al., arXiv:0805.2595.
 - ²⁹ Y. Nakai, K. Ishida, Y. Kamihara, M. Hirano, and H. Hosono, arXiv:0804.4765.
 - ³⁰ H. Mukuda, N. Terasaki, H. Kinouchi, M. Yashima, Y. Kitaoka, S. Suzuki, S. Miyasaka, S. Tajima, K. Miyazawa, P. Shirage, et al., arXiv:0806.3238.
 - ³¹ N. Bulut and D. J. Scalapino, Phys. Rev. Lett. **68**, 706 (1992).

- ³² B. Mitrovic and K. V. Samokhin, Phys. Rev. B **74**, 144510 (2006).
- ³³ H. Kotegawa, K. Ishida, Y. Kitaoka, T. Muranaka, and J. Akimitsu, Phys. Rev. Lett **87**, 127001 (2001).
- ³⁴ D. Parker, O. V. Dolgov, M. M. Korshunov, A. A. Golubov, and I. I. Mazin, arXiv:0807.3729.
- ³⁵ A. V. Chubukov, D. Efremov, and I. Eremin, arXiv:0807.3735.
- ³⁶ Y. Bang and H.-Y. Choi, arXiv:0807.3912.